International Journal of Fluid Power 13 (2012) No. 2 pp. 29-40

NUMERICAL AND EXPERIMENTAL STUDY OF HYDROSTATIC DISPLACEMENT MACHINE

Rasmus Soerensen[1], Michael Hansen[2] and Ole Mouritsen[3]

[1]*Liftra & Aalborg University, Department of Mechanical and Manufacturing Engineering. Karlskogavej 12, 9220 Aalborg SV, Denmark.*
[2]*University of Agder, Department of Engineering. Torvasen 11, 4886 Grimstad, Norway*
[3]*Aalborg University, Department of Mechanical and Manufacturing Engineering. Fibigerstraede 16, 9220 Aalborg East, Denmark.*
rms@liftra.dk, michael.r.hansen@uia.no, oom@m-tech.aau.dk

Abstract

This paper presents a simulation tool to determine the structural deflections and corresponding leakage flow in a hydrostatic displacement motor. The simulation tool is applied to a new motor principle that is categorized as an extreme low speed high torque motor with dimensions that calls for attention to the volumetric efficiency. To counteract structural deflections the motor is equipped with compensation pressure volumes that may be used to limit the leakage flow across the end faces of the circular rotor. This leakage flow is investigated by solving Reynolds equation for the pressure distribution across both end faces. The fluid pressure is combined with structural calculations in a fluid structural interaction simulation which evaluates the influence of structural deflections on the gaps and the leakage flow.

The numerical work is validated by prototype tests. Both deflections and leakage flows are measured and compared with those from the simulations with good correlation. The deflections, and hence leakage flow, are reduced by the use of compensation pressure volumes, which is validated both numerically and experimentally.

Keywords: hydrostatic motor, fluid structure interaction, leakage flow, experimental verification.

1 Introduction

The development and manufacturing of hydraulic motors is both time consuming and expensive due to its strong dependency on tolerances and prototype design. The manufacturing tolerances and surface roughness of the internal parts require special machining facilities and extra manufacturing steps. Also, assembly and testing must be carried out with tight tolerances on parameters such as bolt pretension, choice of fluid and fluid temperature. When developing new motors whether it is a new type of motor or simply scaling of an existing this is even more pronounced. The use of a model based approach to the design is complicated by the fact that two important design criteria; volumetric efficiency and hydromechanical efficiency are difficult to evaluate due to their strong relationship to tribology phenomena. Therefore, the modelling typically requires handling of friction, lubrication and complex structural deflections.

Fluid film lubrication and elastic surface deformations have been of high interest for several researchers and in different applications. In Ivantysynova et al. (2009), Huang et al. (2006), Ivantysynova et al. (2009) and Wieczorek et al. (2002) the lubricating gap of axial piston machines are investigated. The dynamic simulation models in these papers considers, among others, non-isothermal fluid flow, squeeze effect in the lubricating gap due to piston motion and effects due to deformation of parts caused by fluid pressure. The experimental validation is based on measured pressures and temperatures in the lubricating gap. In Manring et al. (2002) and Karadere (2010) the fluid film lubrication and elastic surface deformation of hydrostatic thrust bearings are investigated. The main focus in these two papers is the effects of deformed gap surfaces. Depending on the deformation modes, the load carrying capacity and power costs of a thrust bearing are influenced. In Koç (1990) the numerical solution of the Reynolds equation governing the fluid film of thrust bearings is of concern.

In this paper fluid-structural interaction modelling is used to evaluate a new motor design with emphasis on the external leakage (drain) paths across the end faces of the rotor. This includes an investigation of the effect of using compensation pressure volumes to ma-

This manuscript was received on 1 September 2011 and was accepted after revision for publication on 15 February 2012

nipulate the external leakage paths across the rotor faces.

The aim of the model development is a computational tool that can predict the effects and consequences of an up-scaling or modification of the motor principle, and, subsequently, minimizing the demands for prototyping. The aim is to up-scale the motor to displacements in the range of 200…500 l / rev, for extraordinary low speed high torque applications. Hence, minimization of the leakage paths and the structural deflections are envisaged to be crucial in order to reach useful volumetric efficiencies.

2 Motor Principle

The hydraulic motor principle investigated in this paper is described in Sørensen et al. (2009, 2011). It is categorized as an extreme low speed high torque motor. The volumetric efficiency is critical for slowly rotating motors. In the present motor principle it is especially the leakage flow into the drain that is affecting the volumetric efficiency. The drain is located in the centre and on both sides of the rotor. The oil is flowing into the drain across the end faces of the rotor from the high pressure chambers (see Fig. 1). The rotor is rotating because of pressure difference across the vanes. The stops and the rotor form six chambers that are further divided by either one or two vanes. However, it can be designed with any number of chambers as a trade off between specific displacement (displacement per motor volume) and complexity. The vanes are moved in radial direction when passing a stop. This radial movement of the vanes is actuated by hydraulic pressures which due to the inlet/outlet system are causing an axial force imbalance at the rotor.

The height of the gaps between the moving parts in hydraulic motors is crucial for the efficiency and the performance. These gaps both serve as sliding bearings and leakage paths. Hence, within the entire operational range of the motor these gaps should be capable of securing fluid film lubrication without causing excess leakage flow.

The hydraulic motor principle shown in Fig. 1 has several leakage paths along the vanes and the rotor, but only the lubricating gaps at the end faces of the rotor (between the rotor and the inner housings) are of concern in this paper. The pressure distribution in these lubricating gaps is creating a significant force at the housings because of the large area from the outer radius of the chambers to the drain connections located close to the centre of the rotor. This force is causing a deflection of the inner housings which must be minimized to maximize the volumetric efficiency of the motor. To counteract deflections of the lubricating gap of concern, the motor has compensation pressure volumes between the inner and outer housings (see location of compensation volumes in Fig. 1). All the compensation pressure volumes are enclosed by o-ring sealing, which are, among other details, not illustrated in Fig. 1.

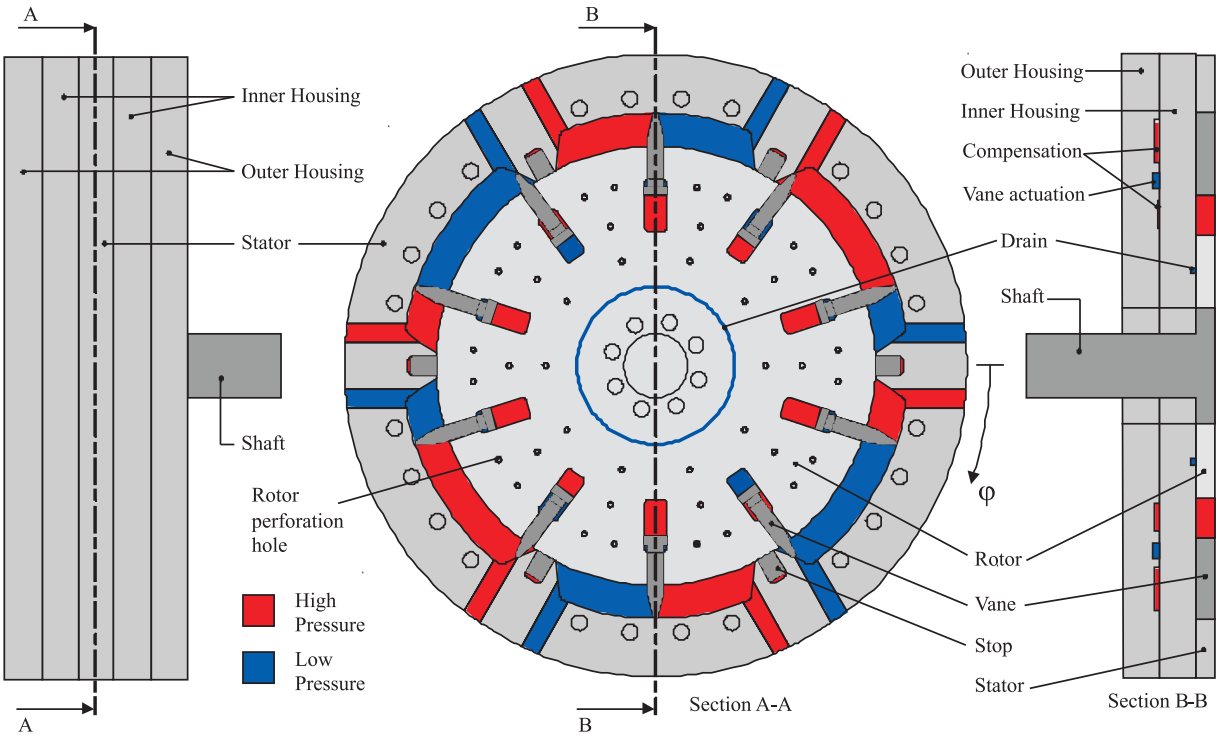

Fig. 1: *Side and end view of motor principle*

3 Fluid Structure Interaction Simulation Model

The fluid structure interaction is handled by using the partitioning approach as defined in Felippa et al. (2001). The fluid and the structural calculations are carried out separately. The discretization is the same for both the structural and the fluid calculations which is easing the interchange of state variables.

3.1 Pressure Distribution in the Gaps Between Rotor and Housings

The pressure distribution in the lubricating gaps between the end faces of the rotor and the inner housings are given by the Reynolds equation for fluid film lubrication.

The general Reynolds equation is (Hamrock et al., 2004)

$$\begin{aligned} 0 = & \frac{\partial}{\partial x}\left(-\frac{\rho \cdot h^3}{12 \cdot \eta} \cdot \frac{\partial p}{\partial x}\right) + \frac{\partial}{\partial y}\left(-\frac{\rho \cdot h^3}{12 \cdot \eta} \cdot \frac{\partial p}{\partial y}\right) \\ & + \frac{\partial}{\partial x}\left(\frac{\rho \cdot h \cdot \left(u_{\mathrm{m}} + u_{\mathrm{n}}\right)}{2}\right) \\ & + \frac{\partial}{\partial y}\left(\frac{\rho \cdot h \cdot \left(v_{\mathrm{m}} + v_{\mathrm{n}}\right)}{2}\right) \\ & + \rho \cdot \left(w_{\mathrm{m}} - w_{\mathrm{n}}\right) - \rho \cdot u_{\mathrm{m}} \cdot \frac{\partial h}{\partial x} \\ & - \rho \cdot v_{\mathrm{m}} \cdot \frac{\partial h}{\partial y} + h \cdot \frac{\partial \rho}{\partial t}, \end{aligned} \tag{1}$$

where subscript m denotes the surface of body m and subscript n denotes the surface of body n (see Fig. 2).

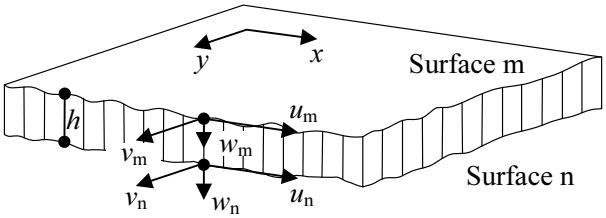

Fig. 2: *Illustration of the fluid film between surface m and surface n*

It is assumed that the rigid body motion of the rotor is rotational and axial and that the density and viscosity of the oil is constant. Furthermore, the Reynolds equation is expressed in polar coordinates, because of the geometry and rotational motion of the rotor. Therefore the pressure distribution in the gaps between the housing and the end faces of the rotor is, refer to (Beschorner et al., 2009; Ivantysynova et al., 2009),

$$\begin{aligned} & \frac{\partial}{\partial r}\left(r \cdot h^3 \cdot \frac{\partial p}{\partial r}\right) + \frac{1}{r} \cdot \frac{\partial}{\partial \theta}\left(h^3 \cdot \frac{\partial p}{\partial \theta}\right) \\ & = 6 \cdot \eta \cdot r \cdot \omega \cdot \frac{\partial h}{\partial \theta} + 12 \cdot \eta \cdot r \cdot \frac{\partial h}{\partial t} \end{aligned} \tag{2}$$

Equation (2) is solved numerically using the finite difference method for one rotor position. By dividing the area into elements (see Fig. 3) and approximating the derivatives in Eq. (2) by finite differences, $p_{\mathrm{i,j}}$ is expressed by its surrounding pressures and can be determined by looping through the mesh until the pressure variation from previous iteration ($p_{\mathrm{i,j}}^{\mathrm{cur}} - p_{\mathrm{i,j}}^{\mathrm{prev}}$) is smaller than a convergence tolerance.

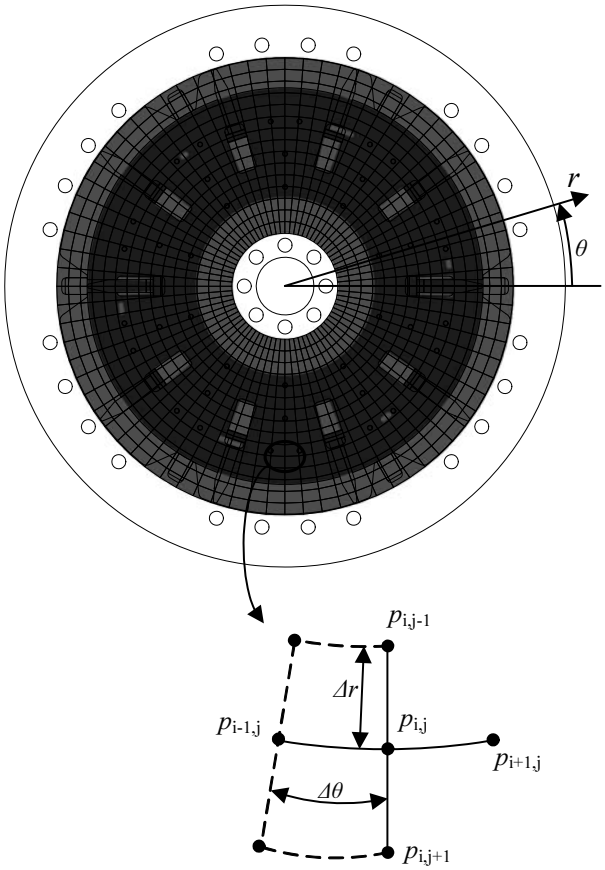

Fig. 3: *Finite difference mesh and boundary conditions. The colour red indicates that the pressure of the node is prescribed whereas blue indicates that the pressure is to be determined in the finite difference analysis*

The rotor is perforated to balance the pressure at each side of the rotor. Therefore a finite difference relaxation is carried out in parallel for both sides of the rotor. For the nodes placed within the area of perforation holes, the pressure is therefore affected by the pressure at the opposite side of the rotor. After solving Eq. (2) for $p_{\mathrm{i,j}}$ at both side of the rotor, the nodes are stated as the mean pressure of the two sides, as

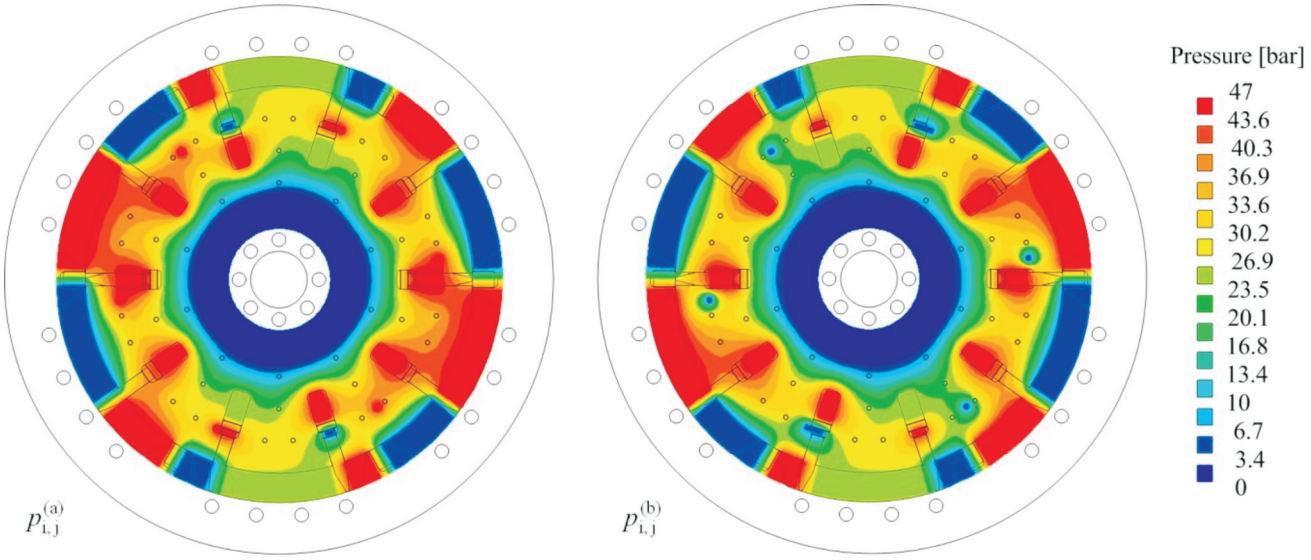

Fig. 4: *The pressure distribution in the lubricating gaps for one rotor position. The gaps are mirrored to each other.* $p_{i,j}^{(a)}$ *is the gap pressure with high pressure connected to the vane actuations and* $p_{i,j}^{(b)}$ *with tank pressure to the vane actuations. The boundary conditions for this pressure distribution is* $p_1 = 47$ *bar in the high pressure side of the vanes,* $p_2 = 6$ *bar in the low pressure side of the vanes and* $p_t = 1$ *bar in the drain connection*

$$p_{i,j}^{(a)} = p_{i,j}^{(a)} - 0.5 \cdot \left(p_{i,j}^{(a)} - p_{i,j}^{(b)} \right) \tag{3}$$

$$p_{i,j}^{(b)} = p_{i,j}^{(b)} - 0.5 \cdot \left(p_{i,j}^{(b)} - p_{i,j}^{(a)} \right), \tag{4}$$

where superscript (a) denotes one end face of the rotor and superscript (b) denotes the other end face of the rotor.

The boundary conditions to this finite difference method are the fixed pressures in the volumes. It is assumed that the pressure decreases linearly across both stops and vanes.

The pressure distribution in the fluid films across the end faces of the rotor for one motor pressure state is illustrated in Fig. 4.

3.2 The Structural Deflections

The objective of the FEM models is to determine the structural deflections of the inner housing and the end face of the rotor which is forming the lubricating gaps of concern (see Fig. 5). The input to the FEM simulations is the pressure distribution in the fluid film and in the compensation volumes and the output is the deflection of the end faces, i.e., the variation of the gap.

The pressure in the compensation volumes is applied as pressures in the FEM simulation, whereas the pressure in the lubricating gap is added as nodal forces. The pressures from the fluid calculations is recalculated as nodal forces by

$$F_{i,j} = p_{i,j} \cdot r_{i,j} \cdot \Delta r \cdot \Delta \theta \tag{5}$$

The total height of the lubricating gap h is influenced by the deflection of the inner housing δ_{housing}, the rotor δ_{rotor} and the initial gap height h_{ini}, given by (see Fig. 5)

$$\Delta h_{i,j} = \delta_{i,j,\text{rotor}} + \delta_{i,j,\text{housing}} \tag{6}$$

$$h_{i,j} = h_{\text{ini}} + \Delta h_{i,j} \tag{7}$$

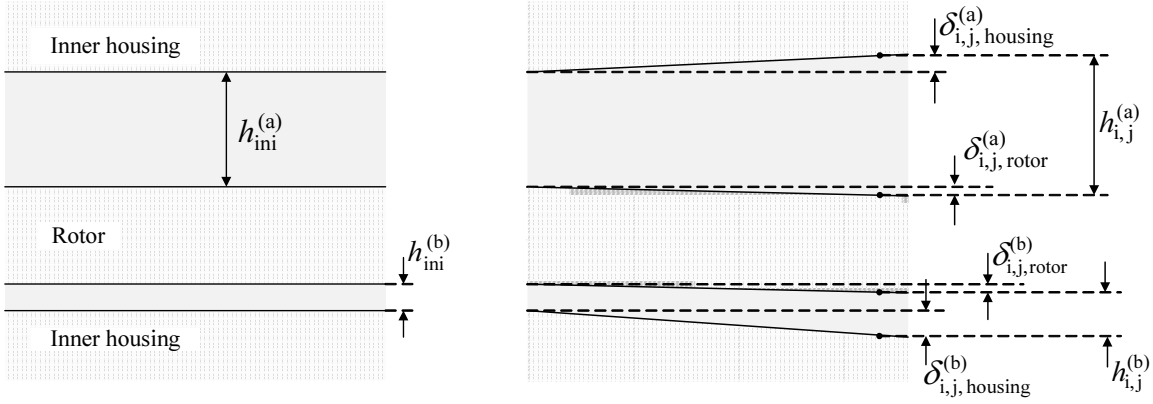

Fig. 5: *Illustration of initial gap and deformed gap*

Different FEM models have been used in the simulations. In Model I both inner housings and the rotor are individual FEM models, see Fig. 6. The output of the FEM analysis is used in the overall fluid-structure analysis. The deflections are used to compute $\Delta h_{i,j}^{(a)}$ and $\Delta h_{i,j}^{(b)}$. The resultant axial force on the rotor introduces an axial rotor velocity, $\delta h / \delta t$ (Eq. (2)). Simulations have shown that changing the rotor to a rigid body in this analysis reduces computational costs and has negligible effect on both pressure distribution and leakage flow across the end faces. The model with rigid rotor is referred to as Model II and has been preferred over Model I because of the reduced computational costs.

As described in the next section on the fluid-structure interaction the rotor position is updated from the $\delta h/\delta t$ term, and, eventually, reaches the inner housing. The rotor is forced against an inner housing due to asymmetry in the vane actuation commutation. As the rotor approaches the inner housing the lubrication film height will become zero (or negative) in certain regions corresponding to structural contact. Because of this Model II (and Model I) can only be used to describe the gap conditions in a satisfactory way up until mechanical contact is observed. In practice, the fluid film remains, however, its behavior in the areas with small or no gap is that of mixed lubrication and should be described by means of more complex models that also include surface details.

When mechanical contact is observed a third model, Model III, is employed where a flexible rotor is connected to the inner housing via contact elements, see Fig. 6. Because of the mixed lubrication conditions, the tangential friction coefficient between the rotor and inner housing is set to $\mu = 0.15$, according to the one used for oil lubricated threat-nut combination in Norton (2000). The mixture of pressure and contact forces between the rotor and the inner housing is now represented by the normal reactive forces of the contact elements.

The different FEM models in Fig. 6 have a number of boundary conditions in common: There are no displacements in the normal direction to the section cut of the stator. The compensation pressure volumes are included between the inner and outer housing. The applied compensation pressures are symbolized by bold red lines between inner and outer housing. The bold red lines at the gap of interest are where all the individual forces in the fluid are applied based on Eq. (5). They are located between the rotor and the inner housing and are reaching from the outer radius of the chambers into the drain connection. The vertical bold red lines symbolize the average chamber pressure on the stator in radial direction.

All the FEM models are meshed by three dimensional 8 node hexahedral elements. The applied mesh for the determination of $\delta_{i,j,\text{housing}}^{(a)}$ is shown in Fig. 7.

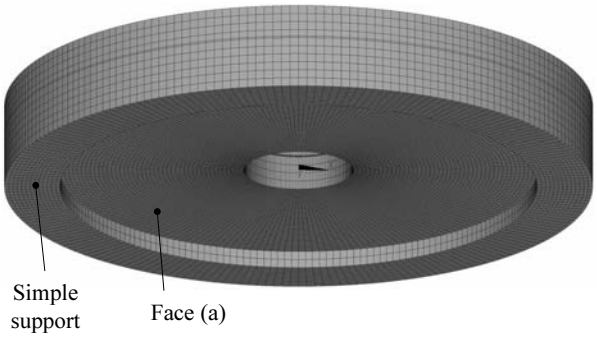

Fig. 6: *The applied mesh for the determination of* $\delta_{i,j,\text{housing}}^{(a)}$. *The FEM mesh consists of three dimensional 8 nodes hexahedral elements*

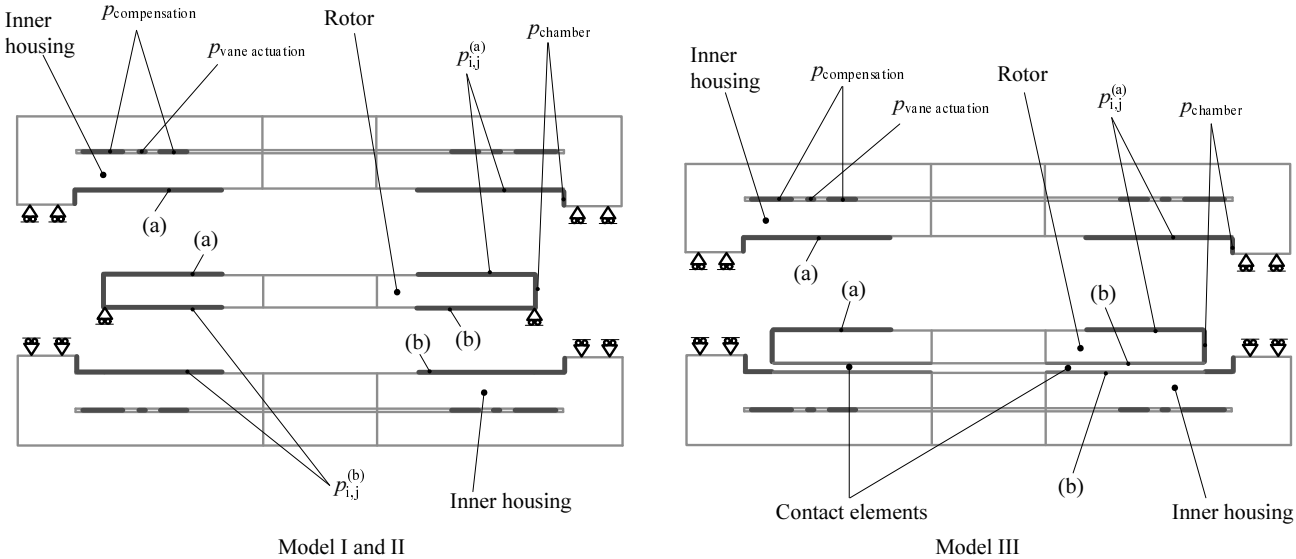

Fig. 7: *The principles behind Model I and II are shown to the left and the principles behind Model III are shown to the right*

3.3 The Interaction Between the Fluid and the Structural Simulations:

The pressure distribution in the lubricating gap is influenced by the gap height and the gap height is influenced by the pressure distribution. To be able to convert node forces from the fluid- to the structural calculations and to convert node deflections from the structural- to the fluid calculations, the node numbering and coordinates are equal.

The simulation model is handling the lubricating gap between the rotor and the inner housing at both side of the rotor. The two sides are analyzed simultaneously to be able to determine the axial position of the rotor and include the effect of the pressure equalizing perforation holes.

The simulation model is illustrated by a flow chart in Fig. 8. Initially all the constants, initial values and boundary conditions are specified. Next step is the initialization of the most outer loop of the simulation model, which is the time loop that updates the part of the gaps that are not influenced by the deflections, $h_{\mathrm{ini}}^{(\mathrm{a})}$ and $h_{\mathrm{ini}}^{(\mathrm{b})}$. The time dependent term, $\partial h / \partial t$ of Eq. (2), is solved for via a Newton Raphson iteration loop, see Fig. 8. Hence, the axial rigid body velocity of the rotor relative to the inner housings is computed in each time step and is used to update the gap heights as

$$h_{\mathrm{ini}}^{\mathrm{cur}} = h_{\mathrm{ini}}^{\mathrm{prev}} + \frac{\partial h}{\partial t} \cdot \Delta t$$

where Δt is the step size of the time integration. Initially, the rotor is in the centre between the inner housings, $h_{\mathrm{ini}}^{(\mathrm{a})} = h_{\mathrm{ini}}^{(\mathrm{b})}$.

The first step in the fluid structure interaction (FSI) loop of the program is to recalculate the node pressures into node forces using Eq. (5). This is carried out in the main Matlab program and the node forces are written to a separate text file in the FEM solver (ANSYS in this study) node force syntax. This text file is the force input to the structural FEM solver analysis. The output from the FEM solver analysis is the node deflection for the nodes that are forming the lubricating gap. These node deflections are again communicated to the main Matlab program in a text file and added to the initial gap heights to express the total gap height for each node location. After the determination of the gap height in the individual nodes, the fluid calculations are performed. For every node Eq. (2) is solved by the finite difference method by looping through the entire mesh. This procedure is continued until the convergence statement is fulfilled.

The last part of the FSI loop is to evaluate the FSI convergence statement. This convergence statement is based on the total change of pressure, compared to the previous FSI iteration with the previous gap heights. When this total change of pressure is sufficiently small, the gap heights and pressures have converged.

The last step in the simulation model is to determine the theoretical external leakage flow based at the determined pressures and gap heights. The leakage flow pr. node is

$$Q_{\mathrm{i,j}} = -\frac{1}{12 \cdot \eta} \cdot h_{\mathrm{i,j}}^{3} \cdot \frac{\partial p_{\mathrm{i,j}}}{\partial r} \cdot r \cdot \Delta\theta$$

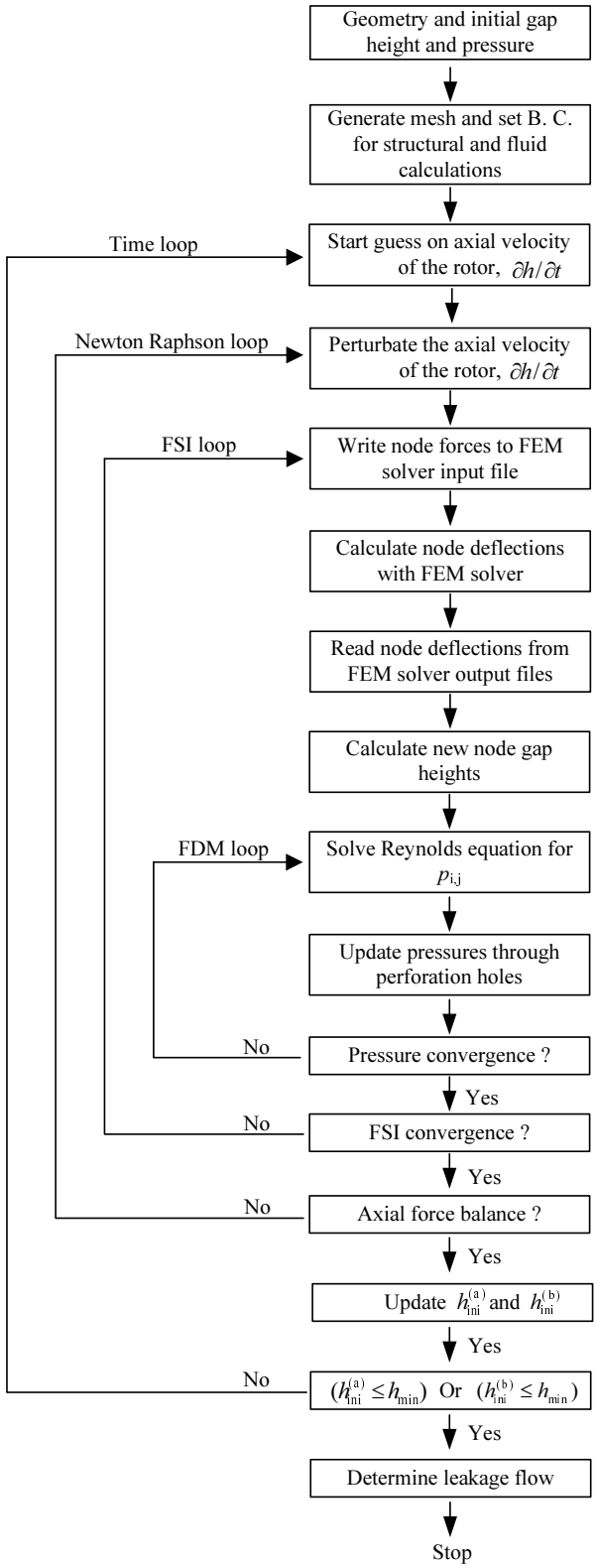

Fig. 8: *The flow chart of the simulation model*

The force imbalance at the rotor in axial direction is balanced by the pressure in the lubricating gaps. In Ivantysynova et al. (2009) force balance for external forces and fluid film pressure is used to determine the gap height of the fluid film between the cylinder block and valve plate in an axial piston machine. Similarly, in Isaksson et al. (2009) the fluid film gap height is modified to balance external forces and fluid film pressure in a radial piston machine.

In the simulation model the axial forces at the rotor is balanced by the squeeze effect in the fluid film until the rotor comes to rest or approaches an inner housing to an extent where the gap height becomes zero (or negative) in certain regions. Then the force balance is obtained by modifying the axial velocity of the rotor ($\partial h / \partial t$ in Eq. (2)). The equations are solved for $\partial h / \partial t$ using the Newton Raphson solver.

The input to the simulation model is measured pressures. The boundary conditions for the simulation model are the pressure state in the high and low pressure volumes around the vanes, which are those governing the pressure distribution in the gap, and the pressure in the compensation volumes. The pressure difference across the vanes depends on the loading of the motor output shaft.

A trend of the simulation model is that the rotor is forced against one of the inner housings and maintains this position steady state. Then the lubricating gap height at the one side of the rotor is maximized and at the other side there is no lubricating gap, but instead mixed film lubrication.

4 Experimental Verification by Prototype Tests

The simulation model is verified by comparing simulated results and measured results. The measured results are generated by doing measurements on a prototype motor.

The data for the prototype motor and the motor conditions during the tests are listed in table 1.

The structural deflections are measured with a moving coil actuator (MCA) that is fitted with a 0.1μm encoder. The body of the MCA is mounted on the inner housing of the prototype motor as illustrated in Fig. 9. The MCA is controlled in force mode and maintains a force of 1.7 N during the test. Then the piston of the MCA is always touching the rotor during tests. The build-in encoder of the MCA is measuring the position of the piston and therefore the relative distance, or deflections, between the housing and the rotor. The measurements are performed when the rotor rotates and therefore the MCA tip is sliding across the face of the rotor. Hence, the output from the MCA is gap heights at a circle of points.

Furthermore, the location of the compensation volumes and the vane actuation connections are shown in the cut through view on Fig. 9.

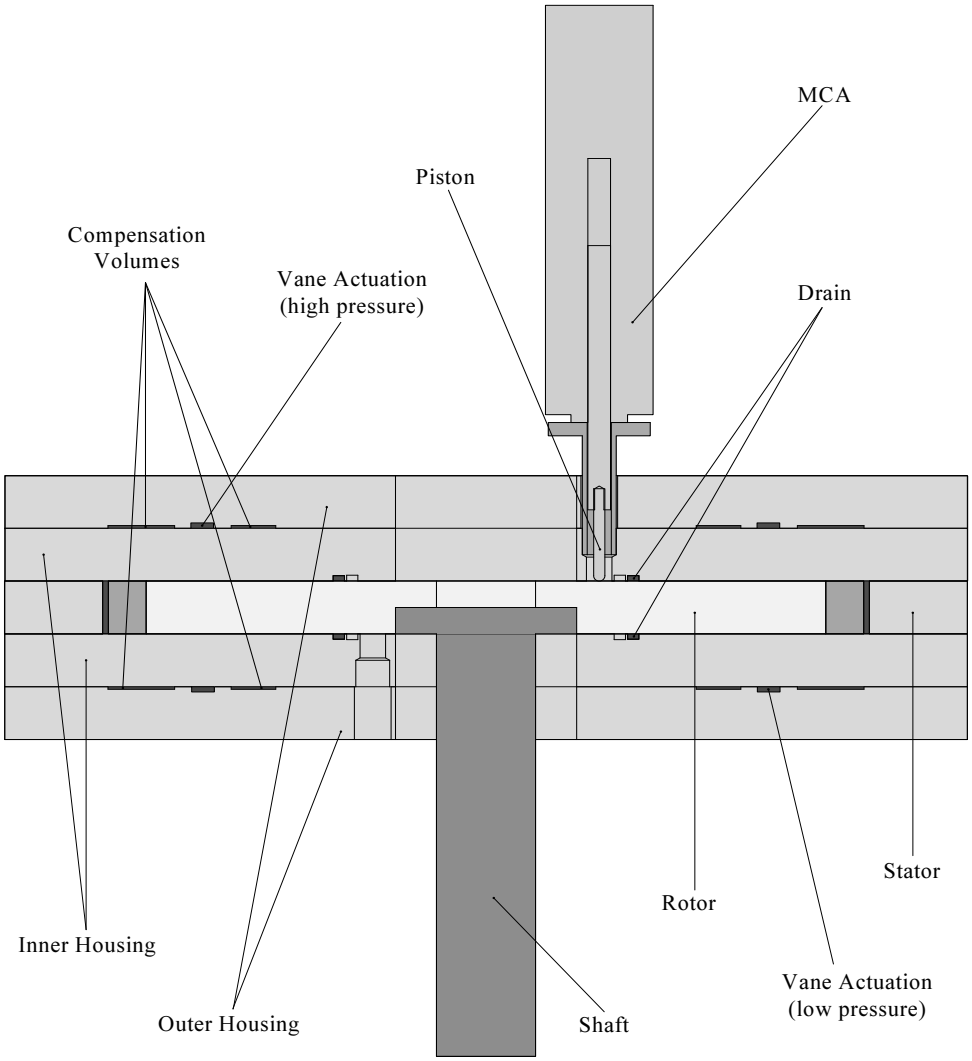

Fig. 9: *The prototype motor in a section cut with compensation volumes and the moving coil actuator mounted*

Table 1: The specifications of the prototype motor and the operating conditions during the tests

Outer motor diameter	$d = 340$ mm
Outer motor height	$L = 100$ mm
Height of rotor	$S = 20$ mm
Number of chambers	$n_{ch} = 6$
Number of vanes	$n_{vane} = 10$
Maximum working pressure during tests	$p_1 = 57$ bar
Prototype displacement	$D = 1.75$ l/rev
Maximum rotational speed during tests	$\omega = 5$ rev/min
Maximum output torque during tests	$T = 1000$ Nm
Input flow during tests	$Q_1 = 10$ l/min

Apart from the MCA the test setup is equipped with flow and pressure transducers. A part of the hydraulic diagram of the test setup is shown in Fig. 10. The oil flow into and out of the motor is measured. The two drain connections are each fitted with a flow transducer to be able to measure the drain flows individually. These two flow transducers are a second option to validate the theoretical simulations because of the relation between the structural deflections and the drain flow. The pressure transducers are measuring the pressure state in the motor during the tests. The measured pressures are the boundary conditions for the theoretical simulations.

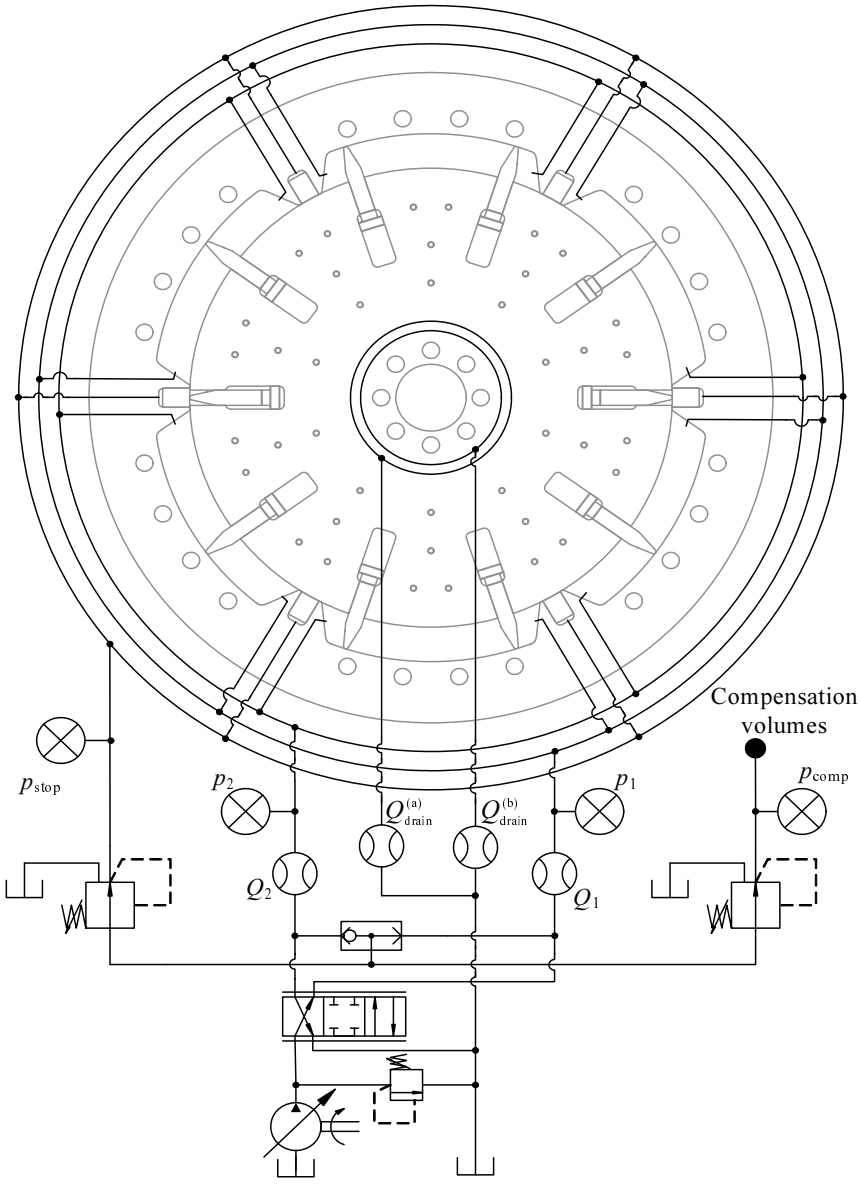

Fig. 10: *A part of the hydraulic diagram of the test setup with pressure and flow transducers and two pressure reducing valves*

The test setup is equipped with a pressure reducing valve to reduce the pressure in the compensation volumes. The pressure reducing valve is adjustable, but the reduction pressure is kept constant at p_{comp} = 35 bar during all the tests. Then the effect of the compensation volumes can be validated by comparing deflections when $p_1 < 35$ bar, i.e. $p_{comp} = p_1$, and when $p_1 > 35$ bar, i.e. $p_{comp} < p_1$.

The prototype motor is loaded by a powder brake, through a gearbox, in the test setup. The resistance torque of the powder brake is electronically adjustable. The torque performance of the prototype motor is measured by strain gauges on the output axle. The angular position and velocity of the motor are measured with an optical encoder mounted on the test setup.

The prototype motor is shown in Fig. 11 in both the test setup and when partly disassembled.

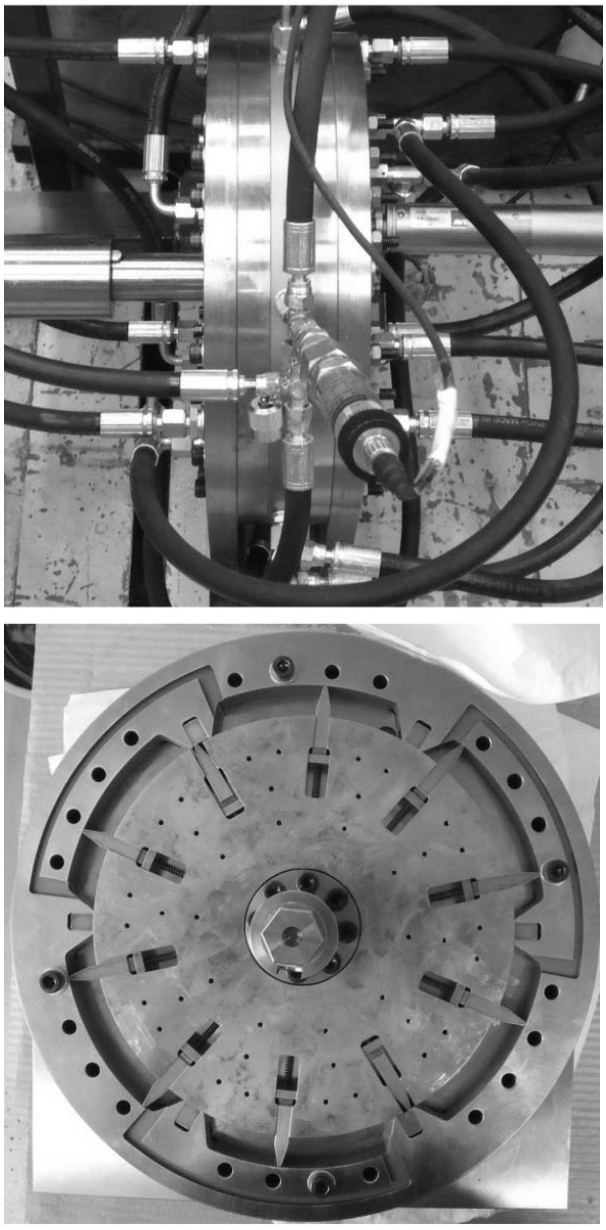

Fig. 11: *The prototype motor in the test setup and when partly assembled*

5 Comparison of Simulated Results and Experimental Results

The experimental results are based on measurements during a considered steady state run. As concluded by the end of section 4, the rotor of the prototype is forced against one of the inner housing, which is the case until the rotational direction of the motor is changed. Therefore rigid body motion of the rotor in axial direction is not handled in the experimental measurements or the result comparison.

The loading of the motor and the input flow are kept constant during a test run and the mean values are extracted from the measurement devices. This procedure is continued to generate all the test data, by only changing the resistance torque of the powder brake. By changing the resistance torque the high pressure, and hence deflections and drain flow, become different for the individual test sequences. The input flow to the motor is kept constant during all the measurements.

The measured deflections and drain flows are extracted to a representative time point for all the different load cases. The simulated results are based at one fixed rotor angle, which approximately represents the mean theoretical drain flow. This rotor angle is the one used in Fig. 3, Fig. 4 and Fig. 10.

In Fig. 12 to the left both the simulated and measured deflection of the gap are plotted with respect to the high pressure p_1. There is no rigid body motion included on the graph. Both the measured and simulated curves in Fig. 12 have a bend at 35bar, which is the pressure limit for the compensation pressure p_{comp} as controlled by the pressure reducing valve. The reason for reducing the compensation pressure is to be able to investigate the effect on the deflection. The vertical axis is gap deflection as described by Eq. (6). The simulated deflections are showing a good correlation with the measured deflections.

The simulated deflections do not completely follow one path because of variations in the measured p_{comp} and p_2 to the same measured p_1. These pressures are input to the simulation model, which then is causing variations in the simulated Δh to the same p_1.

The deflection curves are not intersecting in Δh=0. The reason is the significant measured p_2 pressures which are above tank pressure.

The measured and simulated drain flows $Q_{drain}^{(a)}$ with respect to h are shown in Fig. 12 to the right. All the point marks are measured and simulated flows during a considered steady state test sequence. In all the measurements the corresponding drain flow $Q_{drain}^{(b)}$ and gap height $h^{(b)}$ are zero, due to the axial force imbalance on the rotor.

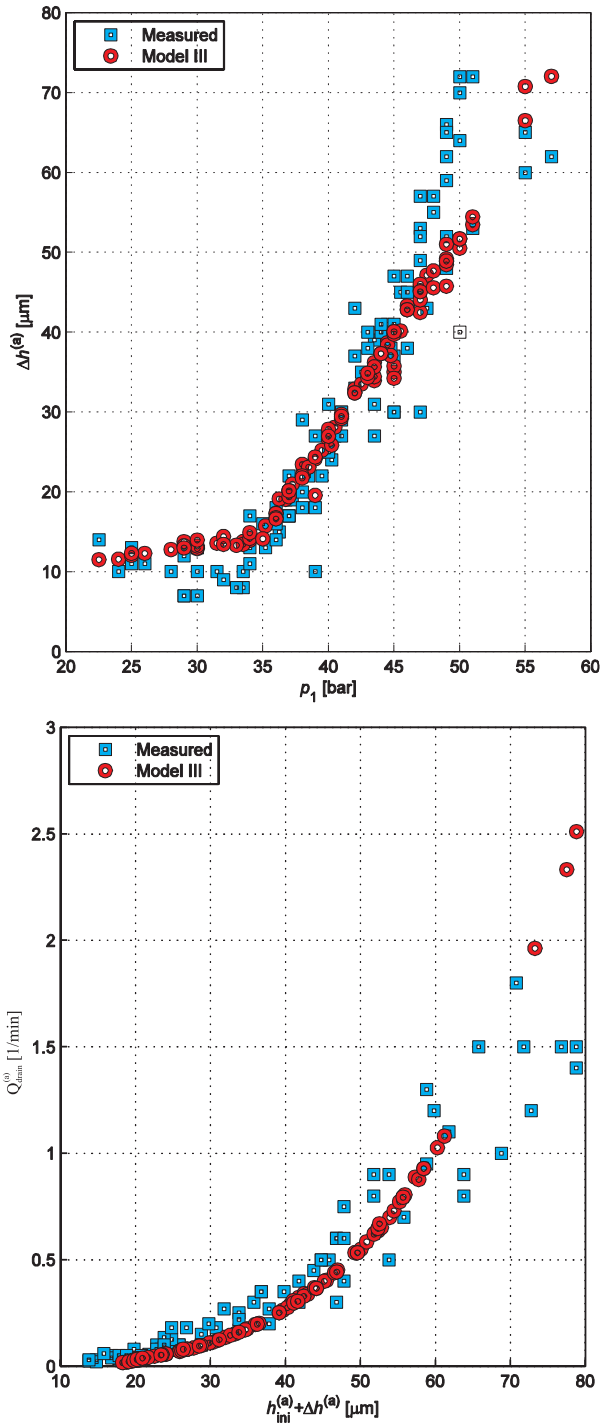

Fig. 12: *To the upper is measured and simulated deflection with respect to the measured high pressures and to the lower is leakage flow with respect to the total gap height*

6 The Effect of Axial Balancing of the Rotor

To quantify the effect of the compensation volumes onto the external leakage flow, the individual external leakage flows are determined by the simulation model (see Fig. 13). The upper graph is showing the external leakage flow of the motor with no compensation pressures. It is plotted with respect to p_1. The second graph is the drain flow for the motor with compensation pressures. The compensation pressure is not restricted by a pressure reducing valve, which means that $p_{comp} = p_1$ to every load situations in Fig. 13. The effect of the compensation pressures on Q_{drain} is remarkable. This trend has also been demonstrated experimentally, but the measurements are not useful for a comparison. The prototype gets unsteady or unable to rotate without the use of the compensation pressures, because of too much volumetric loss.

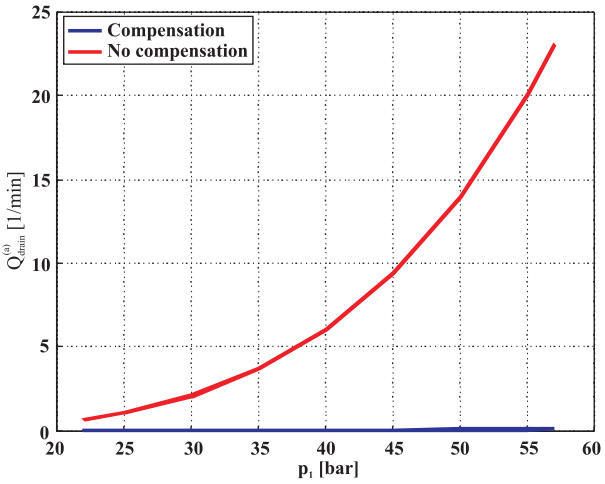

Fig. 13: *The effect of the compensation pressure volumes on the drain flow. The graphs are showing the drain flow with and without compensation pressures*

7 Conclusions

The lubricating gap height and leakage flow are determined by employing different fluid structure interaction simulation models. The basic simulation model (Model I) determines the pressure distribution in the lubricating gaps between the rotor and the inner housing by solving Reynolds equation and determines the structural deflections of the surfaces that form the gap by FEM simulations. Furthermore, the Model I computes the axial velocity of the rotor that generates force equilibrium due to the squeeze effect. A somewhat simpler model (Model II) neglects the flexibility of the rotor. Both models converge towards a situation where the rotor comes in structural contact with the inner housing leading to a third model (Model III) where the mixed lubrication regime between rotor and inner housing are modelled as a frictional contact model. This model seems to be in good accordance with the experimental data, especially regarding the measured structural deflections. This validates the simulation model which is targeted to serve as a design tool when up-scaling the motor.

The combined numerical and experimental investigation carried out on a prototype of the new motor principle reveals that the leakage gaps caused by elastic deformations can be prevented by the use of pressure compensation volumes. The elastic deformations of the hydrostatic motor principle put forward in this paper can be kept at an acceptable level by the use of compensation volumes. They both save material costs and improve the compactness of the motor. This is especially significant for larger motors.

Nomenclature

d	Diameter	[m]
D	Displacement	[m^3/rev]
F	Force	[N]
h	Gap height	[m]
l	Outer motor height	[m]
n_{ch}	Number of chambers	[]
n_{vane}	Number of vanes	[]
p	Pressure	[Pa]
Q	Flow	[m^3/s]
r	Radius, radial coordinate	[m]
s	Height of rotor	[m]
T	Torque	[Nm]
t	Time	[s]
u	Velocity along x axis	[m/s]
v	Velocity along y axis	[m/s]
w	Velocity along z axis	[m/s]
x	Cartesian coordinate	[m]
y	Cartesian coordinate	[m]
δ	Structural deflection	[m]
Δh	Total gap deflection	[m]
Δp	Pressure difference	[Pa]
Δr	Radial element division	[m]
Δt	Time step	[s]
$\Delta\theta$	Tangential element division	[rad]
η	Dynamic viscosity	[Pa s]
θ	Angular coordinate	[rad]
μ	Coefficient of friction	[]
ρ	Density	[kg/m^3]
φ	Angular position	[rad]
ω	Angular velocity	[rad/s]

References

Beschorner, K., **Higgs III, C. F.** and **Lovell, M.** 2009. Solution of Reynolds Equation in Polar Coordinates Applicable to Nonsymmetric Entrainment Velocities. *Journal of Tribology*. Vol 131.

Felippa, C. A., **Park, K. C.** and **Farhat, C.** 2001. Partitioned analysis of coupled mechanical systems. *Computer Methods in Applied Mechanics and Engineering.* Vol 190.

Hamrock, B. J., **Schmid, S. R.** and **Jacobsen, B. O.** 2004. *Fundamentals of Fluid Film Lubrication*. 2. Edition. s.l. : Marcel Dekker Inc.

Huang, C. and **Ivantysynova, M.** 2006. An Advanced Gap Flow Model Considering Piston Micro Motion and Elastohydrodynamic Effect. *Proc. of the 4th FPNI PhD Symposium, Sarasota*.

Isaksson, P., Nilsson, D. and Larsson, R. 2009. Elasto-hydrodynamic simulation of complex geometries in hydraulic motors. *Tribology International 42*.

Ivantysynova, M. and **Baker, J.** 2009. Power loss in the lubricating gap between cylinder block and valve plate of swash plate type axial piston machines. *International Journal of Fluid Power*. No. 2.

Ivantysynova, M. and **Pelosi, M.** 2009. A novel fluid-structure interaction model for lubricating gaps of piston machines. *Fluid Structure Interaction V*.

Karadere, G. 2010. The effects of the total bearing deformation on the performance of hydrodynamic thrust bearings. *Industrial Lubrication and Tribology*. Vol 62.

Koç, E. 1990. An investigation into the numerical solution of Reynolds' lubrication equation with special reference to thrust bearings. *Tribology International*. Vol 23.

Manring, N. D., **Johnson, R. E.** and **Cherukuri, H. P.** 2002. The Impact of Linear Deformations on Stationary Hydrostatic Thrust Bearings. *Journal of Tribology*. Vol 124.

Norton, R. L. 2000. *MACHINE DESIGN An Integrated Design*. s.l. : Prentice Hall.

Soerensen, R. M., et al. 2011. Hydraulic Yaw System for Wind Turbines with New Compact Hydraulic Motor Principle. *Proc. of the European Wind Energy Association Conference, Bruxelles*.

Soerensen, R. M., et al. 2009. Investigation of Hydraulic Motor Principle for Low Speed High Torque Applications. *Proc. of the 22th. Nordic Seminar on Computational Mechanics, Aalborg*.

Wieczorek, U. and **Ivantysynova, M.** 2002. Computer Aided Optimization og Bearing and Sealing Gaps in Hydrostatic Machines - The Simulation Tool CASPER. *International Journal of Fluid Power* 1.

Rasmus Moerk Soerensen
Rasmus Moerk Soerensen graduated as a M.Sc. in mechanical engineering from Aalborg University in 2008. He is employed at Liftra as an industrial PhD. The PhD project is in collaboration between Liftra and Department of Mechanical and Manufacturing Engineering at Aalborg University. His research area is related to modelling of a hydrostatic motor and prototype testing.

Michael Hansen
Since 2009 the author is Professor in Fluid Power at the Department of Engineering at the University of Agder and also a part-time research engineer at Aker Solutions AS. His primary interests are hydraulic and mechanical machine dynamics. He has an M.Sc in mechanical engineering from Aalborg University and a Ph.D. in computer based simulation and design of mechanical mechanisms.

Ole O. Mouritsen
Ole O. Mouritsen received his M.Sc. from the Technical University of Denmark, 1970. He is employed as Associate Professor at Aalborg University, Department of Mechanical and Manufacturing Engineering since 1985. He previously worked at the Danish Engineering Academy, Odense Steel Shipyard Ltd. and The Danish Welding Institute (FORCE). His research interests include machine elements, FEM calculations, fatigue and fracture mechanics.